Inorganic Chemistry

Article

pubs.acs.org/IC

New Molybdenum(VI) Phosphates: Synthesis, Characterization, and Calculations of Centrosymmetric $RbMoO_2PO_4$ and Noncentrosymmetric $Rb_4Mo_5P_2O_{22}$

Ying Wang,[†,‡] Shilie Pan,*[,†] Xin Su,[†] Zhihua Yang,*[,†] Lingyun Dong,[†,‡] and Min Zhang[†]

[†]Xinjiang Key Laboratory of Electronic Information Materials and Devices, Xinjiang Technical Institute of Physics & Chemistry, Chinese Academy of Sciences, 40-1 South Beijing Road, Urumqi 830011, China

[‡]University of Chinese Academy of Sciences, Beijing 100049, China

Supporting Information

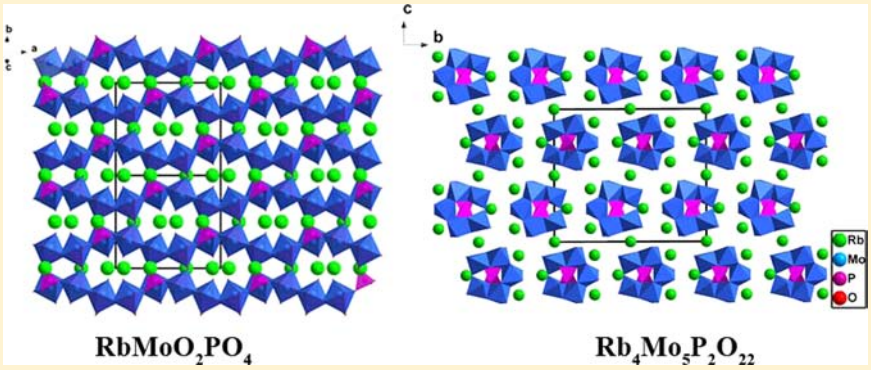

ABSTRACT: Two new molybdenum(VI) phosphates, $RbMoO_2PO_4$ and $Rb_4Mo_5P_2O_{22}$, have been synthesized by standard solid-state reactions, and their structures were determined by single-crystal X-ray diffraction. The former is centrosymmetric, whereas the latter is noncentrosymmetric and chiral. Their crystal structures both consist of corner- and edge-shared MoO_6 octahedra, PO_4 tetrahedra, and RbO_n (n = 8 or 10) polyhedra and exhibit three- and one-dimensional structures, respectively. Powder second-harmonic generation (SHG) measurements revealed an SHG efficiency of approximately 1.4 × KH_2PO_4 (KDP) for $Rb_4Mo_5P_2O_{22}$. Thermal analysis, infrared and UV−vis-NIR diffuse reflectance spectroscopy, and electronic band structure calculations were also performed on the reported materials. Crystal data are the following: $RbMoO_2PO_4$, orthorhombic, space group *Fddd* (No. 70), a = 11.012(5) Å, b = 12.403(5) Å, c = 15.839(7) Å, V = 2163.3(16) Å^3, and Z = 16; $Rb_4Mo_5P_2O_{22}$, orthorhombic, space group $C222_1$ (No. 20), a = 6.5300(5) Å, b = 19.7834(18) Å, c = 17.3451(15) Å, V = 2240.7(3) Å^3, and Z = 4.

INTRODUCTION

Noncentrosymmetric (NCS) oxide materials are of current interest and great importance attributable to their functional properties, such as ferroelectricity, piezoelectricity, and second-harmonic generation (SHG).[1] To design and synthesize new NCS materials, various strategies have been published. For example, Chen's group has successfully used π-conjugated planar borate rings to direct new NCS borate-based materials with enhanced SHG responses.[2] Halasyamani et al. have prepared many new NCS and polar oxide materials based on cations that are susceptible to second-order Jahn−Teller (SOJT) distortions.[3] Significant research efforts have been focused on compounds containing stereochemically active lone-pair cations.[4] Recently, our group has reported a series of materials with strong SHG efficiencies by incorporating the alkali cations and halide anions into the borate system.[5]

Here, we are interested in introducing octahedrally coordinated d^0 transition-metal cations (Ti^{4+}, Nb^{5+}, Mo^{6+}, W^{6+}, etc.) to the metal phosphate systems in order to enhance their SHG properties. With the magnitude, the Mo^{6+} has the largest SOJT distortion scales among transition-metal cations,[6] which has been demonstrated to be a good candidate to design new NCS materials with excellent SHG properties.[7] Besides, metal phosphates exhibit a wide variety of compositions and structural versatility,[8] and a large number of NCS materials have been discovered in this system, such as KH_2PO_4 (KDP),[9] $KTiOPO_4$ (KTP),[10] $KNd(PO_3)_4$,[11] etc. Thus, the combination of MoO_6 and PO_4 groups may lead to the formation of unique structures and high SHG efficiencies. In addition, it is expected that the molybdophosphate heteropolyanions, namely, polyoxometalates with multiple highly distorted MoO_6 octahedra and PO_4 tetrahedra polymerized into polynuclear clusters, may

Received: October 14, 2012
Published: January 15, 2013

   dx.doi.org/10.1021/ic302246c | *Inorg. Chem.* 2013, 52, 1488−1495

exhibit larger polarizations. However, SHG properties of such materials are seldom discovered.[12]

In this paper, we report on the synthesis and characterization of two new molybdenum(VI) phosphates: centrosymmetric $RbMoO_2PO_4$ and noncentrosymmetric $Rb_4Mo_5P_2O_{22}$. Interestingly, $RbMoO_2PO_4$ exhibits a structure related to gismondine (GIS), and $Rb_4Mo_5P_2O_{22}$ displays a novel structure derived from Strandberg-type polyoxometalate. In addition to the crystal structures, thermal behavior, spectrum, SHG properties, and electronic band structure calculations of the title compounds were also described.

EXPERIMENTAL SECTION

Reagents. All commercially available chemicals (Rb_2CO_3, Cs_2CO_3, MoO_3, and $NH_4H_2PO_4$) are of reagent grade and were used as received.

Syntheses. Small single crystals of $RbMoO_2PO_4$ and $Rb_4Mo_5P_2O_{22}$ were grown by spontaneous crystallization. A mixture of 0.115 g (0.5 mmol) of Rb_2CO_3, 0.144 g (1.00 mmol) of MoO_3, and 0.115 g (1.00 mmol) of $NH_4H_2PO_4$ for $RbMoO_2PO_4$ and a mixture of 0.462 g (2.00 mmol) of Rb_2CO_3, 0.720 g (5.00 mmol) of MoO_3, and 0.230 g (2.00 mmol) of $NH_4H_2PO_4$ for $Rb_4Mo_5P_2O_{22}$ were thoroughly ground. The respective mixtures were then placed in a platinum crucible that was placed into a vertical, programmable-temperature furnace. The crucible was gradually heated to 780 °C in air, held for 12 h, and then slowly cooled down to 400 °C at a rate of 3 °C·h^{-1}, followed by rapid cooling to room temperature. Moreover, $RbMoO_2PO_4$ could also be successfully obtained via a high-temperature solution method under similar conditions. A mixture of a 0.346 g (1.50 mmol) portion of Rb_2CO_3, 0.163 g (0.50 mmol) of Cs_2CO_3, 0.720 g (5.00 mmol) of MoO_3, and 0.230 g (2.00 mmol) of $NH_4H_2PO_4$ was used as the starting material. The addition of Cs_2CO_3 acts as the flux and helps the crystallization. For $RbMoO_2PO_4$, yellow-green block crystals were found, whereas for $Rb_4Mo_5P_2O_{22}$, yellow block crystals were recovered. The crystals were separated mechanically from the crucible for the further characterization by single-crystal X-ray measurements.

Polycrystalline samples of $RbMoO_2PO_4$ and $Rb_4Mo_5P_2O_{22}$ were synthesized via conventional solid-state reactions. A separate stoichiometric mixture of Rb_2CO_3, MoO_3, and $NH_4H_2PO_4$ was initially ground well. The samples were placed in alumina crucibles and heated to 650 °C (520 °C for $Rb_4Mo_5P_2O_{22}$), held for 3 days, and then cooled to room temperature. The purity of the samples was confirmed by a powder X-ray diffraction (XRD) study. Since isostructural compounds of $RbMoO_2PO_4$ are abundant,[13] we also attempted to synthesize the Na^+ and K^+ analogues for $Rb_4Mo_5P_2O_{22}$ but were unsuccessful. However, we have successfully obtained $Cs_4Mo_5P_2O_{22}$ as the isostructural compound of $Rb_4Mo_5P_2O_{22}$ and will publish this work soon.

Single-Crystal X-ray Diffraction. Block crystals of $RbMoO_2PO_4$ (0.087 mm × 0.10 mm × 0.178 mm) and $Rb_4Mo_5P_2O_{22}$ (0.044 mm × 0.087 mm × 0.186 mm) were used for single-crystal data collection. Data were collected on a Bruker SMART APEX II CCD diffractometer using monochromatic Mo Kα radiation (λ = 0.71073 Å) at 293(2) K and integrated with the SAINT program.[14] The numerical absorption corrections were carried out using the SADABS program[15] for area detector. All calculations were performed with programs from the SHELXTL crystallographic software package.[16] The structures were solved by direct methods, and all of the atoms were refined using full-matrix least-squares techniques with anisotropic thermal parameters and final converged for $I > 2\sigma$. The structures were checked for missing symmetry elements with PLATON.[17] The Flack parameter for $Rb_4Mo_5P_2O_{22}$ was refined to 0.017(7). Crystal data and structure refinement information are summarized in Table 1. The selected bond distances are listed in Table 2. The final refined atomic positions and isotropic thermal parameters are given in Table S1 in the Supporting Information.

Powder X-ray Diffraction. Powder XRD data of polycrystalline materials were obtained on a Bruker D2 PHASER diffractometer with Cu Kα radiation (λ = 1.5418 Å) at room temperature. The 2θ range was 5−70° with a step size of 0.02° and a fixed counting time of 1s/step. No impurities were observed, and the experimental powder XRD patterns shown are in good agreement with the calculated ones derived from the single-crystal data (Figure S1 in the Supporting Information).

Thermal Analysis. Thermal gravimetric analysis (TGA) and differential scanning calorimetry (DSC) were carried out on a NETZSCH STA 449C instrument at a temperature range of 50−900 °C with a heating rate of 5 °C·min^{-1} in an atmosphere of flowing N_2.

Vibrational Spectroscopy. IR spectroscopy was carried out on a Shimadzu IR Affinity-1 spectrometer in the 500−4000 cm^{-1} range with a resolution of 4 cm^{-1}. The sample was mixed thoroughly with dried KBr (5 mg of the sample and 500 mg of KBr).

UV−vis-NIR Diffuse-Reflectance Spectroscopy. UV−vis-NIR diffuse-reflectance data were collected with a SolidSpec-3700DUV spectrophotometer using polytetrafluoroethylene as a standard in the wavelength range from 190 to 2600 nm. Reflectance spectra were

Table 1. Crystallographic Data for $RbMoO_2PO_4$ and $Rb_4Mo_5P_2O_{22}$

	$RbMoO_2PO_4$	$Rb_4Mo_5P_2O_{22}$
fw	1425.28	1235.52
crystal system	orthorhombic	orthorhombic
space group	*Fddd* (No. 70)	$C222_1$ (No. 20)
a (Å)	11.012(5)	6.5300(5)
b (Å)	12.403(5)	19.7834(18)
c (Å)	15.839(7)	17.3451(15)
V (Å^3)	2163.3(16)	2240.7(3)
Z	16	4
ρ_{calcd} (g/cm^3)	3.787	3.662
μ (mm^{-1})	11.616	11.592
$2\theta_{max}$ (deg)	27.41	27.55
R (int)	0.0224	0.0515
GOF (F^2)	1.170	0.991
flack parameter		0.017(7)
$R(F)^a$	0.0227	0.0281
$R_w(F_o^2)^b$	0.0623	0.0445

$^aR(F) = \sum||F_o| - |F_c||/\sum|F_o|$. $^bR_w(F_o^2) = [\sum_w(F_o^2 - F_c^2)^2/\sum_w(F_o^2)^2]^{1/2}$.

Table 2. Selected Bond Distances (Å) for $RbMoO_2PO_4$ and $Rb_4Mo_5P_2O_{22}$

$RbMoO_2PO_4$			
Mo(1)−O(3)	1.693(3)	P(1)−O(2)	1.518(3)
Mo(1)−O(3)	1.693(3)	P(1)−O(2)	1.518(3)
Mo(1)−O(1)	1.986(3)	P(1)−O(1)	1.553(3)
Mo(1)−O(1)	1.986(3)	P(1)−O(1)	1.553(3)
Mo(1)−O(2)	2.199(3)		
Mo(1)−O(2)	2.199(3)		
$Rb_4Mo_5P_2O_{22}$			
Mo(1)−O(6)	1.697(4)	Mo(3)−O(12)	1.696(3)
Mo(1)−O(7)	1.707(4)	Mo(3)−O(10)	1.705(4)
Mo(1)−O(5)	1.919(3)	Mo(3)−O(11)	1.905(1)
Mo(1)−O(8)	1.945(4)	Mo(3)−O(5)	1.912(3)
Mo(1)−O(2)	2.243(3)	Mo(3)−O(1)	2.352(3)
Mo(1)−O(4)	2.346(3)	Mo(3)−O(2)	2.441(3)
Mo(2)−O(9)	1.703(3)	P(1)−O(1)	1.497(4)
Mo(2)−O(9)	1.703(4)	P(1)−O(4)	1.524(4)
Mo(2)−O(8)	1.904(3)	P(1)−O(2)	1.531(3)
Mo(2)−O(8)	1.904(3)	P(1)−O(3)	1.593(2)
Mo(2)−O(4)	2.289(3)		
Mo(2)−O(4)	2.289(3)		

dx.doi.org/10.1021/ic302246c | Inorg. Chem. 2013, 52, 1488−1495

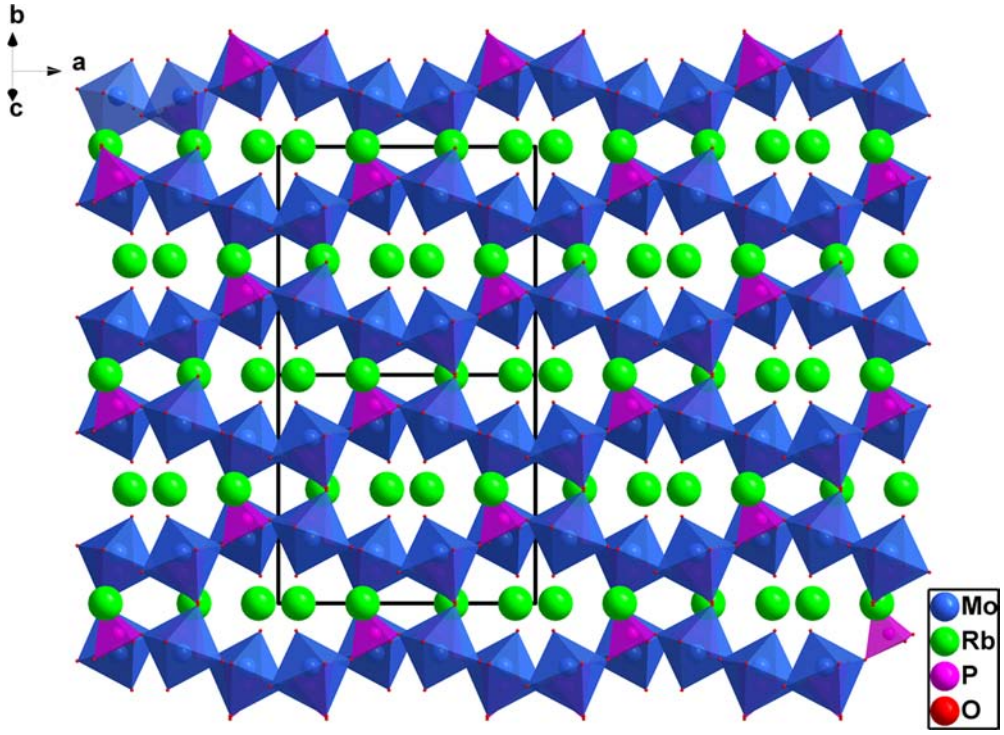

Figure 1. Polyhedra representation of $RbMoO_2PO_4$ along the [011] direction.

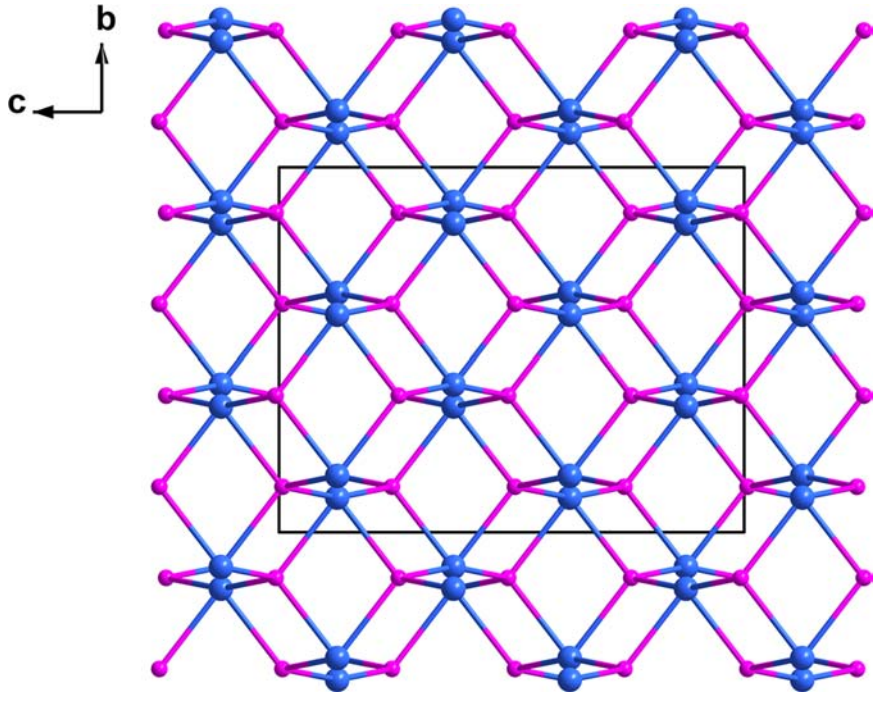

Figure 2. Topological view of the $4^3.4^2.8$ net of $RbMoO_2PO_4$. MoO_6 (light blue spheres) and PO_4 (purple spheres) groups are viewed as two kinds of 4-connected nodes.

converted to absorbance using the function, $F(R) = (1 - R)^2/2R$, where R is the reflectance and $F(R)$ is the Kubelka–Munk remission function.[18]

Second-Order Nonlinear Optical Measurements. Powder SHG measurements were performed on a modified Kurtz–Perry system[19] using a pulsed Nd:YAG laser with a wavelength of 1064 nm. A detailed description of the equipment and the methodology used has been published.[20] Because the SHG efficiency has been shown to depend on particle size,[21] polycrystalline samples were ground and sieved into distinct particle size ranges: <20, 20–38, 38–55, 55–88, 88–105, 105–150, 150–200, and 200–250 μm. Microcrystalline KDP were also ground and sieved into the same particle size ranges and served as a reference. Powders with particle sizes of 105–150 μm were used for comparing SHG intensities.

Computational Details. First-principles density functional theory (DFT) electronic structure calculations for the two compounds were performed with the total-energy code CASTEP.[22] The exchange-correlation effects were treated with the general gradient approx-

dx.doi.org/10.1021/ic302246c | Inorg. Chem. 2013, 52, 1488–1495

imation (GGA) using the Perdew–Burke–Ernzerhof (PBE) functional.[23] The interactions between the ionic cores and the electrons were described by the ultrasoft pseudopotentials.[24] The Monkhorst–Pack scheme *k*-point grid sampling was set at 3 × 3 × 3 in the primitive cell of the Brillouin zone (BZ) for the total energy calculations. The plane-wave cutoff energy was set to 540.0 eV, which proved to be an optimal level of the total energy convergence. The following orbital electrons were treated as valence electrons: Rb, $4p^6 5s^1$; Mo, $4p^6 4d^5 5s^1$; P, $3s^2 3p^3$; and O, $2s^2 2p^4$. The other parameters used in the calculations were set by the default values of the CASTEP code.

RESULTS AND DISCUSSION

Structure of $RbMoO_2PO_4$. Crystallographic analysis revealed that $RbMoO_2PO_4$ belongs to the space group *Fddd* with an asymmetric unit consisting of one unique rubidium atom, one unique molybdenum atom, one unique phosphorus atom, and three unique oxygen atoms (Table S1 in the Supporting Information). The structure of $RbMoO_2PO_4$ features a complicated three-dimensional (3D) $[MoO_2PO_4]^-$ framework composed of distorted MoO_6 octahedra and PO_4 tetrahedra, containing tunnels running along the crystallographic *a* axis in which the Rb^+ ions reside (Figure 1). In this framework, the MoO_6 octahedra share four of their corners with PO_4 tetrahedra, and the other two corners are free. In a topological view, since two terminal oxygen atoms of MoO_6 are not involved in the formation of the 3D topological structure, MoO_6 and PO_4 groups can be both viewed as 4-connected nodes. As shown in Figure 2, the topology of the $[MoO_2PO_4]^-$ framework could be described as a (4, 4)-connected double-nodal GIS type[25] network, with a Schläfli notation $(4^3.4^2.8)$[26] or named as an *sqc* net in the Reticular Chemistry Structure Resource (RCSR) database.[27] An edge-type (local *C*2 direction) distortion is observed for each MoO_6 octahedron, with two "short" (1.692(3) Å), two "intermediate" (1.968(3) Å), and two "long" (2.199(3) Å) Mo–O bonds. In the PO_4 tetrahedra, each P atom is coordinated by four O atoms, forming a PO_4 distorted tetrahedron with two kinds of P–O bonds (1.518(3) and 1.553(3) Å). The Rb atoms are surrounded by 10 oxygen atoms with distances ranging from 2.906(3) to 3.373(3) Å. In connectivity terms, the structure of $RbMoO_2PO_4$ may also be written as $\{[MoO_{4/2}O_{2/1}]^{2-}[PO_{4/2}]^+\}^-$ with the charge balanced by the Rb^+ cation. Bond valence calculations[28] resulted in values of 1.15, 6.10, and 4.99 for Rb^+, Mo^{6+}, and P^{5+}, respectively (Table 3).

Table 3. Bond Valence Sum (vu), Bond Strain Index (BSI), and Global Instability Index (GII) of $RbMoO_2PO_4$ and $Rb_4Mo_5P_2O_{22}$.

	bond valence sum				
compound	Rb^+	Mo^{6+}	P^{5+}	BSI	GII
$RbMoO_2PO_4$	1.15	6.10	4.99	0.10	0.10
$Rb_4Mo_5P_2O_{22}$	0.79–1.43	6.06–6.21	4.99	0.08	0.14

The discovery of $RbMoO_2PO_4$ has filled up the blank of the $AMoO_2PO_4$ (A = univalent cation) series compounds.[13] Therefore, a comparison of these compounds is worth doing and is as below: $NaMoO_2PO_4$[13a] and $AgMoO_2PO_4$[13b] are isostructural and crystallize in the space group $P2_1/c$, whereas $KMoO_2PO_4$,[13c] $RbMoO_2PO_4$, $CsMoO_2PO_4$, and $TlMoO_2PO_4$[13d] are isostructural and belong to the space group *Fddd*. For the latter, the molecular volumes (*V* unit cell/*Z*) increase linearly with larger cationic radius: 132.2 $Å^3$ (K) < 134.0 $Å^3$ (Tl) < 135.2 $Å^3$ (Rb) < 138.5 $Å^3$(Cs). Besides, the anionic framework of $NaMoO_2PO_4$ and $AgMoO_2PO_4$ is quite different from the K–Cs and Tl series.[13d] Although the coordination geometry of the anionic polyhedra is almost the same for all compounds in this series, the environments of univalent cations are different. For small cations, Na^+ and Ag^+, they are only interacted with six oxide ligands, whereas larger coordination environments are required for K^+, Rb^+, Cs^+, and Tl^+ cations. Thus, the coordination requirements of the cation will determine the final structure of the material.[29]

Structure of $Rb_4Mo_5P_2O_{22}$. X-ray analysis revealed that $Rb_4Mo_5P_2O_{22}$ belongs to the space group $C222_1$. Three unique rubidium atoms, 3 unique molybdenum atoms, 1 unique phosphorus atom, and 12 unique oxygen atoms are in an asymmetric unit (Table S1 in the Supporting Information). $Rb_4Mo_5P_2O_{22}$ exhibits 1D $_\infty[Mo_5P_2O_{22}]^{4-}$ anion chains that are separated by Rb^+ cations (Figure 3). The fundamental structure of the $_\infty[Mo_5P_2O_{22}]^{4-}$ chain is the diphosphopentamolybdate $[Mo_5P_2O_{23}]^{6-}$ unit, which could be described as a ring formed by five distorted edge- or corner-shared MoO_6 octahedra, capped by two PO_4 tetrahedra from either side (Figure 5e). This kind of structure is a typical Strandberg-type unit[30] and could be found in many other polyoxometalate compounds.[31] The units are further covalently connected by a P–O–P linker, forming a 1D infinite chain along the crystallographic *a* axis. The chains are arranged in an antiparallel manner and are slightly shifted along [010] to obtain the stacking crystal structure (Figure 4). There are three symmetry-independent Mo atoms located in severely distorted octahedral environments attributable to SOJT effects. Each of the three Mo atoms is shifted toward an edge of its oxide octahedron (local C_2 [110] direction), resulting in two "short" Mo–O bonds (1.696(3)–1.707(4) Å), two "intermediate" bonds (1.904(3)–1.945(4) Å), and two "long" bonds (2.243(3)–2.441(3) Å). The tetrahedral coordinated P atoms have P–O distances in the range of 1.497(4)–1.593(2) Å. Three different RbO_n (n = 8 or10) polyhedra are observed with the Rb–O bonds distances ranging from 2.775(4) to 3.491(4) Å. In connectivity terms, the structure of $Rb_4Mo_5P_2O_{22}$ may also be written as $\{2[MoO_{2/1}O_{3/2}O_{1/3}]^{1.667-}2[MoO_{2/1}O_{2/2}O_{2/3}]^{1.333-}[MoO_{2/1}O_{2/2}O_{2/3}]^{1.333-}2[PO_{2/2}O_{2/3}]^{1.667+}\}^{4-}$ with the charge balanced by the Rb^+ cation. Bond valence calculations[28] resulted in values of 0.79–1.43, 6.02–6.21, and 4.99 for Rb^+, Mo^{6+}, and P^{5+}, respectively (Table 3).

$Rb_4Mo_5P_2O_{22}$ is a new type of Strandberg-type polyoxometalate derivative. Because the P–O–P linkers, namely, diphosphate units, exist, it can be classified as a molybdenum diphosphate. Accordingly, its formula can also be written as $Rb_4[(P_2O_7)Mo_5O_{15}]$. Many molybdenum diphosphates have been discovered; however, to our best knowledge, this kind of $[(P_2O_7)Mo_5O_{15}]^{4-}$ chain structure has not been described before.

Octahedral Distortion, Local Dipole Moments, Bond Strain Index (BSI), and Global Instability Index (GII). All of the MoO_6 octahedra in $RbMoO_2PO_4$ and $Rb_4Mo_5P_2O_{22}$ distort along the local C_2 [110] direction. We can quantify the magnitude of this distortion using the method proposed by Halasyamani.[6b] The obtained magnitude of the Mo^{6+} distortion (Δ_d) values for the MoO_6 octahedra in $RbMoO_2PO_4$ is 1.03. The values for three unique MoO_6 octahedra in $Rb_4Mo_5P_2O_{22}$ are 1.28, 1.21, and 1.42, respectively (Table 4). These values indicate that all MoO_6 octahedra belong to the type of strong

dx.doi.org/10.1021/ic302246c | Inorg. Chem. 2013, 52, 1488–1495

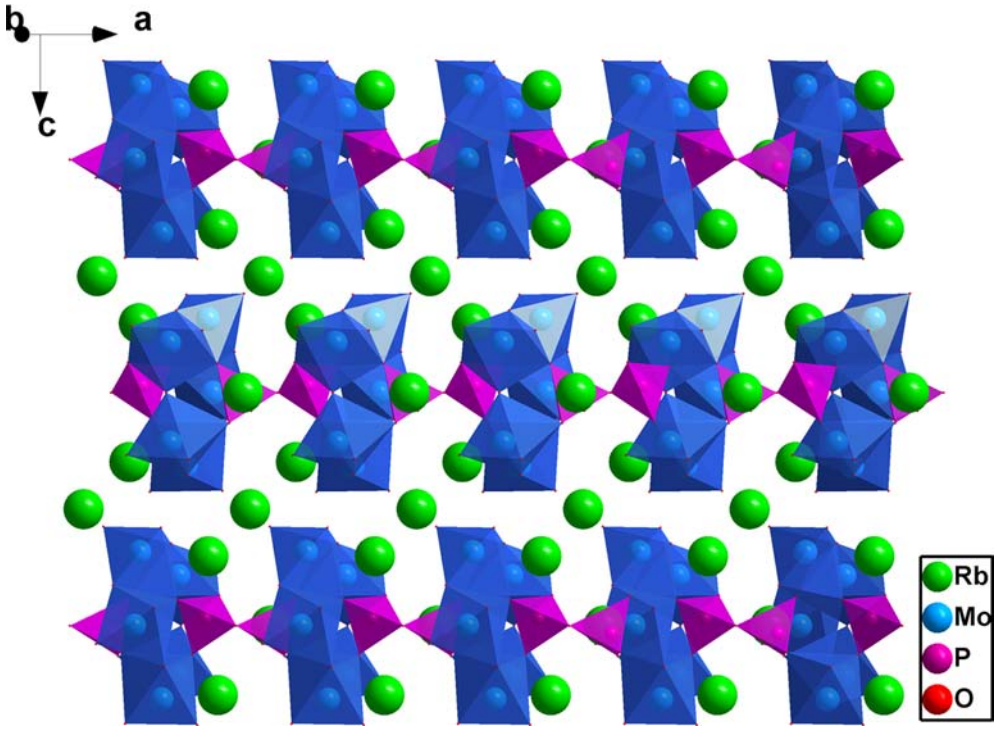

Figure 3. Polyhedra representation of $Rb_4Mo_5P_2O_{22}$ along the [110] direction.

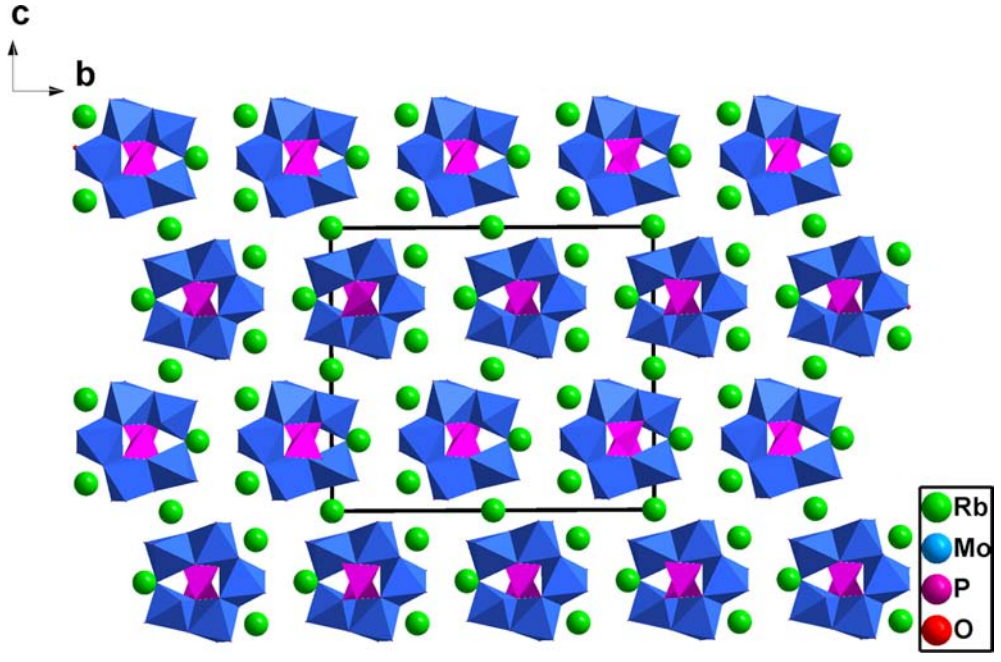

Figure 4. Polyhedra representation of $Rb_4Mo_5P_2O_{22}$ along the [100] direction. The $[Mo_5P_2O_{23}]^{6-}$ chains are arranged in an antiparallel manner and are slightly shifted along the [010] direction.

distortion (Δ_d > 0.8), and the distortions in $Rb_4Mo_5P_2O_{22}$ are larger than the one in $RbMoO_2PO_4$.

We also examined the direction and magnitude of the local dipole moments for the MoO_6, PO_4, and RbO_n (n = 8 or 10) polyhedra using a bond valence approach.[32] Because both of the compounds are not polar, the net dipole moments of all polyhedra in the unit cell are zero. As summarized in Table 4, although these polyhedra in both compounds have similar coordination environments, the values of local dipole moments for each cation are quite different. The results show that the local dipole moments of RbO_n polyhedra in $RbMoO_2PO_4$ are larger than those in $Rb_4Mo_5P_2O_{22}$. This is not surprising since the Rb^+ cation in the former is located in a larger cavity (GIS-type structure), requiring greater distortion.[33] The calculations for MoO_6 octahedra resulted in values of 0.88−6.71 D, which is consistent with previously reported values,[4b,7a−c] except the one in $RbMoO_2PO_4$. The rather small result for the MoO_6 octahedron in $RbMoO_2PO_4$ could be attributed to its highly symmetrical distorted structure (see Figure 3). Moreover, for $Rb_4Mo_5P_2O_{22}$, we also calculated the total dipole moments of

dx.doi.org/10.1021/ic302246c | Inorg. Chem. 2013, 52, 1488−1495

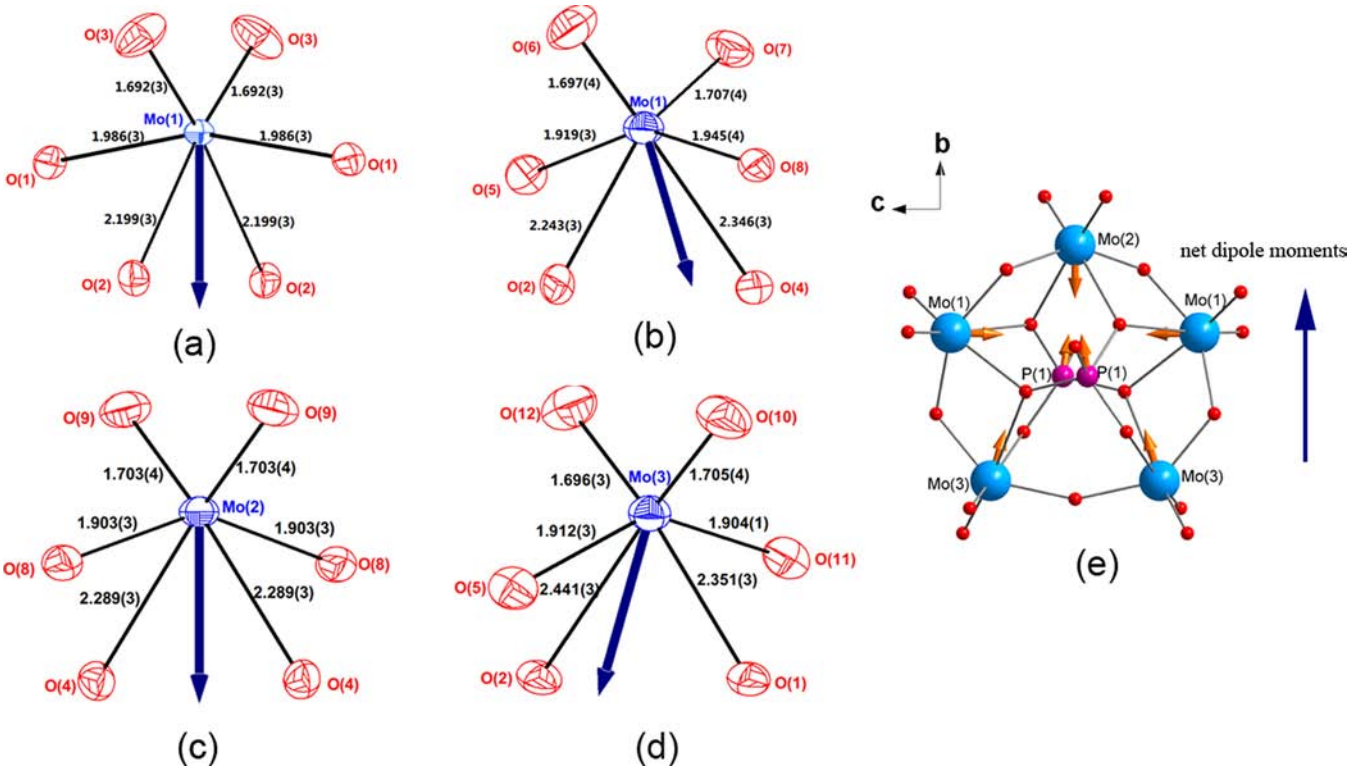

Figure 5. Direction of the local dipole moments for polyhedra. ORTEP (50% probability ellipsoids) drawings of (a) MoO_6 polyhedra in $RbMoO_2PO_4$ and (b–d) MoO_6 polyhedra in $Rb_4Mo_5P_2O_{22}$. (e) Ball-and-stick representation of Strandberg-type unit in $Rb_4Mo_5P_2O_{22}$. The orange and dark blue arrows indicate the approximate direction of the dipole moments.

Table 4. Distortion Magnitudes ($\triangle d$) of MoO_6 Octahedra and Dipole Moments of RbO_n (n = 8 or 10), MoO_6, and PO_4 Polyhedra in $RbMoO_2PO_4$ and $Rb_4Mo_5P_2O_{22}$

		MoO_6 distortion		
compounds		direction	magnitude	polyhedral dipole moment (Debye)
$RbMoO_2PO_4$	$Rb(1)O_{10}$			6.80
	$Mo(1)O_6$	C_2 [110]	1.03	0.88
	PO_4			2.15
$Rb_4Mo_5P_2O_{22}$	$Rb(1)O_{10}$			3.54
	$Rb(2)O_8$			3.25
	$Rb(3)O_{10}$			3.16
	$Mo(1)O_6$	C_2 [110]	1.28	6.71
	$Mo(2)O_6$	C_2 [110]	1.21	6.19
	$Mo(3)O_6$	C_2 [110]	1.42	6.07
	PO_4			2.89
	$[Mo_5P_2O_{23}]^{6-}$			8.96

$[Mo_5P_2O_{23}]^{6-}$ units. Despite the partly cancellation of polarizations from the five neighboring MoO_6 octahedra and the PO_4 tetrahedra, the net dipole moments of $[Mo_5P_2O_{23}]^{6-}$ units are still nonzero (8.96 D, along the [010] direction).

In addition, two structural parameters derived from bond valence concepts, which are the BSI and GII,[34] were calculated (Table 3). A large BSI is indicative of electronic-induced strains; that is, electronic anisotropies originated from the SOJT effect, whereas large GII values are indicative of the lattice-induced strains. BSI and GII values greater than 0.05 vu (valence unit) reveal that the structure is strained, and the structure is unstable with values greater than 0.20 vu. As seen in Table 3, the BSI values of two compounds are very similar (0.08 −0.10 vu). Since the BSI for both compounds is attributable to SOJT distorted Mo^{6+} cations, it is reasonable to expect the BSI values to be similar. For $RbMoO_2PO_4$, the BSI value is as large as the GII value; however, for $Rb_4Mo_5P_2O_{22}$, the GII > BSI, indicating that the lattice-induced strain is stronger than the electronic strain. According to bond valence calculations, the large GII value for $Rb_4Mo_5P_2O_{22}$ is mainly caused by a certain amount of overbonding and underbonding of Rb^+ cations.

Thermal Analysis. The thermal behaviors of $RbMoO_2PO_4$ and $Rb_4Mo_5P_2O_{22}$ are similar (Figure S2 in the Supporting Information). As shown in the TGA curves, both compounds are thermally stable up to high temperatures with nearly no weight loss. Meanwhile, only one endothermic peak was observed from the heating curves of the DSC results (715 and 569 °C for $RbMoO_2PO_4$ and $Rb_4Mo_5P_2O_{22}$, respectively). These endothermic peaks were later pointed out to be the melting points by heating up the two compounds to the corresponding temperatures. In addition, powder samples of the two compounds were put into a platinum crucible, then heated to 780 °C to melt completely, and slowly cooled to room temperature. The powder XRD patterns of before and after melting are identical (Figure S1 in the Supporting Information). Note that the intensity differences between the after melting and calculated patterns are caused by the preferred orientation of the powder sample. From the above discussion, we can draw a conclusion that the two compounds melt congruently.

Spectroscopic Studies. The IR spectra for $RbMoO_2PO_4$ and $Rb_4Mo_5P_2O_{22}$ are shown in Figure S3 in the Supporting Information. For the two compounds, the IR spectra show no

dx.doi.org/10.1021/ic302246c | Inorg. Chem. 2013, 52, 1488–1495

absorption bands in the IR region of 4000−1200 cm^{-1}. Several characteristic absorption bands are observed in the ranges of 940−890 cm^{-1} for Mo−O stretches and 1180−960 cm^{-1} for P−O stretches, respectively. As for $Rb_4Mo_5P_2O_{22}$, the bands around 1174 and 1083 cm^{-1} are assigned to the asymmetric stretches of the P_2O_7 group, further confirming the presence of P−O−P bridges. All of these assignments are consistent with those reported earlier.[35] The UV−vis-NIR diffuse reflectance spectrum for the two compounds reveal that both $RbMoO_2PO_4$ and $Rb_4Mo_5P_2O_{22}$ are insulators with optical band gaps around 2.96 and 3.51 eV, respectively (Figure S4 in the Supporting Information).

SHG Measurements. Because $Rb_4Mo_5P_2O_{22}$ is acentric, it is worth studying its SHG properties. Powder SHG measurements using 1064 nm radiation revealed that the SHG efficiencies of $Rb_4Mo_5P_2O_{22}$ are approximately 1.4 × KDP in the 105−150 μm particle size range (Figure 6). As was

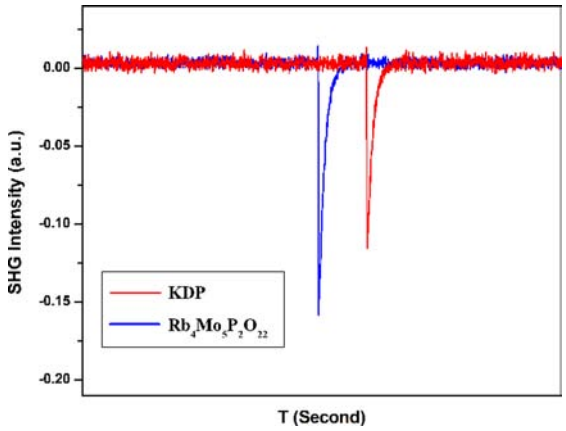

Figure 6. Oscilloscope traces of the SHG signals for the powder (105−150 μm particle size range) of KDP and $Rb_4Mo_5P_2O_{22}$.

previously stated, the Strandberg-type $[Mo_5P_2O_{23}]^{6-}$ anionic units have large local dipole moments; thus, the SHG responses may be attributed to the alignment of these asymmetric units. In addition, the measurements of SHG efficiency as a function of particle size indicated that $Rb_4Mo_5P_2O_{22}$ is type I nonphase-matchable (Figure S5 in the Supporting Information), which falls into the Class C of SHG materials, as defined by Kurtz and Perry.[19]

Electronic Band Structures. Electronic structure calculations were performed in order to examine their band structures as well as to better understand the relationship between electronic structures and optical properties. The electronic band structures of $RbMoO_2PO_4$ and $Rb_4Mo_5P_2O_{22}$ were determined using the plane-wave pseudopotential calculations. The calculated band structures of $RbMoO_2PO_4$ and $Rb_4Mo_5P_2O_{22}$ along high symmetry points of the first Brillouin zone are plotted in Figure S6 in the Supporting Information. It is found that the highest energy of the valence bands (VBs) is localized at the G point for both compounds, whereas the lowest of the conduction bands (CBs) is localized at the Z point with a band gap of 2.825 eV for $RbMoO_2PO_4$, and at the Y point with a band gap of 3.283 eV for $Rb_4Mo_5P_2O_{22}$. Therefore, both compounds are indirect band-gap insulators. The calculated band gaps of both compounds are slightly smaller than the experimental band gaps (2.96 eV for $RbMoO_2PO_4$ and 3.51 eV for $Rb_4Mo_5P_2O_{22}$). The underestimation of the energy gap is typical because the GGA does not accurately describe the eigenvalues of the electronic states, especially for insulators.[36] As seen from the total and partial densities of states (TDOS, PDOS) analyses (Figure S7 in the Supporting Information), both compounds have similar electronic structures except for small differences in the O contributions. For both compounds, the CBs above the Fermi level are mainly derived from Mo 4d orbitals and O 2p orbitals. Meanwhile, they all exhibited three VBs, one each in the lower (below −22.5 eV), middle (from −22.5 to −15 eV), and upper (from −10.5 to 0 eV) energy regions below the Fermi level. In the lower and middle regions, the energy bands are composed mostly of Rb 5s and O 2s orbitals. The upper region arises from mostly Rb 4p, Mo 4d, and O 2p orbitals. In addition, a relatively small contribution from P 3s and P 3p was observed in the electronic structures. From the PDOS calculations, we can state that the band gaps of the two compounds are dominated by the hybridizations of Mo 4d and O 2p orbitals. The similarity in electronic structures of the two compounds may be ascribed to almost the same coordination environments of Rb^+, Mo^{6+}, and P^{5+} cations.

CONCLUSION

Two new molybdenum phosphates, $RbMoO_2PO_4$ (*Fddd*) and $Rb_4Mo_5P_2O_{22}$ ($C222_1$), have been successfully synthesized and characterized. Although the two compounds are synthesized under similar conditions, crystallographic data indicate that $RbMoO_2PO_4$ is centrosymmetric with a 3D framework structure related to GIS, whereas $Rb_4Mo_5P_2O_{22}$ is NCS with a 1D chain structure consisting of Strandberg-type units. Powder SHG measurements on $Rb_4Mo_5P_2O_{22}$ indicate that the material is not phase-matchable (Type 1), with an SHG efficiency ∼ 1.4 times that of KDP. We are in the process of synthesizing other similar quaternary oxide compounds and will be reporting on them shortly.

ASSOCIATED CONTENT

Supporting Information

X-ray data in CIF format, atomic coordinates and equivalent isotropic displacement parameters, powder XRD patterns, TGA and DSC diagrams, IR and UV−vis-NIR diffuse-reflectance spectra, phase-matching diagrams, and electronic band structures patterns. This material is available free of charge via the Internet at http://pubs.acs.org.

AUTHOR INFORMATION

Corresponding Author

*Phone: (86)991-3674558. Fax: (86)991-3838957. E-mail: slpan@ms.xjb.ac.cn (S.P.), zhyang@ms.xjb.ac.cn (Z.Y.).

Notes

The authors declare no competing financial interest.

ACKNOWLEDGMENTS

This work is supported by the National Key Basic Research Program of China (Grant No. 2012CB626803), the "National Natural Science Foundation of China" (Grant Nos. U1129301, 51172277, 21101168, 11104344), the Main Direction Program of Knowledge Innovation of Chinese Academy of Sciences (Grant No. KJCX2-EW-H03-03), the "One Hundred Talents Project Foundation Program" of Chinese Academy of Sciences, the Major Program of Xinjiang Uygur Autonomous Region of China during the 12th Five-Year Plan Period (Grant No. 201130111), and the "High Technology Research and

Development Program" of Xinjiang Uygur Autonomous Region of China (Grant No. 201116143).

REFERENCES

(1) (a) Lines, M. E.; Glass, A. M. *Principles and Applications of Ferroelectrics and Related Materials*; Oxford University Press: Oxford, U.K., 1991; p 576. (b) Cady, W. G. *Piezoelectricity: An Introduction to the Theory and Applications of Electromechanical Phenomena in Crystals*; Dover: New York, 1964; p 822. (c) Munn, R. W.; Ironside, C. N. *Principles and Applications of Nonlinear Optical Materials*; Blackie Academic & Professional: Glasgow, U.K., 1993. (d) Halasyamani, P. S.; Poeppelmeier, K. R. *Chem. Mater.* **1998**, *10*, 2753. (e) Ok, K. M.; Chi, E. O.; Halasyamani, P. S. *Chem. Soc. Rev.* **2006**, *35*, 710.

(2) (a) Chen, C.-T. *Acta Phys. Sin.* **1979**, *22*, 756. (b) Chen, C.-T.; Wu, Y.-C.; Jiang, A.-D.; You, G.-M.; Li, R.-K.; Lin, S.-J. *J. Opt. Soc. Am. B* **1989**, *6*, 616. (c) Chen, C.-T.; Wu, Y.-C.; Li, R.-K. *Int. Rev. Phys. Chem.* **1989**, *8*, 65. (d) Chen, C.-T.; Wang, Y.-B.; Wu, B.-C.; Wu, K.-W.; Yu, L.-H. *Nature* **1995**, *373*, 322. (e) Chen, C.-T.; Lin, Z.-S.; Wang, Z.-Z. *Appl. Phys. B: Lasers Opt.* **2005**, *80*, 1.

(3) (a) Porter, Y.; Halasyamani, P. S. J. *Solid State Chem.* **2003**, *174*, 441. (b) Muller, E. A.; Cannon, R. J.; Sarjeant, A. N.; Ok, K. M.; Halasyamani, P. S.; Norquist, A. J. *Cryst. Growth Des.* **2005**, *5*, 1913. (c) Chang, H.-Y.; Kim, S.-W.; Halasyamani, P. S. *Chem. Mater.* **2010**, *22*, 3241. (d) Yeon, J.; Kim, S.-H.; Halasyamani, P. S. *Inorg. Chem.* **2010**, *49*, 6986. (e) Nguyen, S. D.; Kim, S.-H.; Halasyamani, P. S. *Inorg. Chem.* **2011**, *50*, 5215.

(4) (a) Li, F.; Hou, X.-L.; Pan, S.-L.; Wang, X.-A. *Chem. Mater.* **2009**, *21*, 2846. (b) Nguyen, S. D.; Halasyamani, P. S. *Inorg. Chem.* **2012**, *51*, 9529. (c) Sun, C.-F.; Hu, C.-L.; Xu, X.; Ling, J.-B.; Hu, T.; Kong, F.; Long, X.-F.; Mao, J.-G. *J. Am. Chem. Soc.* **2009**, *131*, 9486. (d) Yu, H.-W.; Pan, S.-L.; Wu, H.-P.; Zhao, W.-W.; Zhang, F.-F.; Li, H.-Y.; Yang, Z.-H. *J. Mater. Chem.* **2012**, *22*, 2105. (e) Zhang, W.-L.; Cheng, W.-D.; Zhang, H.; Geng, L.; Lin, C.-S.; He, Z.-Z. *J. Am. Chem. Soc.* **2010**, *132*, 1508.

(5) (a) Wu, H.-P.; Pan, S.-L.; Poeppelmeier, K. R.; Li, H.-Y.; Jia, D.-Z.; Chen, Z.-H.; Fan, X.-Y.; Yang, Y.; Rondinelli, J. M.; Luo, H. *J. Am. Chem. Soc.* **2011**, *133*, 7786. (b) Yu, H.-W.; Wu, H.-P.; Pan, S.-L.; Yang, Z.-H.; Su, X.; Zhang, F.-F. *J. Mater. Chem.* **2012**, *22*, 9665. (c) Zhang, M.; Pan, S.-L.; Fan, X.-Y.; Zhou, Z.-X.; Poeppelmeier, K. R.; Yang, Y. *CrystEngComm* **2011**, *13*, 2899.

(6) (a) Ok, K. M.; Halasyamani, P. S.; Casanova, D.; Llunell, M.; Alemany, P.; Alvarez, S. *Chem. Mater.* **2006**, *18*, 3176. (b) Halasyamani, P. S. *Chem. Mater.* **2004**, *16*, 3586.

(7) (a) Chi, E. O.; Ok, K. M.; Porter, Y.; Halasyamani, P. S. *Chem. Mater.* **2006**, *18*, 2070. (b) Zhang, J.; Zhang, Z.; Sun, Y.; Zhang, C.; Zhang, S.; Liu, Y.; Tao, X. *J. Mater. Chem.* **2012**, *22*, 9921. (c) Zhang, J.; Zhang, Z.; Zhang, W.; Zheng, Q.; Sun, Y.; Zhang, C.; Tao, X. *Chem. Mater.* **2011**, *23*, 3752. (d) Ok, K. M.; Orzechowski, J.; Halasyamani, P. S. *Inorg. Chem.* **2003**, *43*, 964. (e) Zhang, W.; Li, F.; Kim, S.-H.; Halasyamani, P. S. *Cryst. Growth Des.* **2010**, *10*, 4091.

(8) (a) Van Wazer, J. R.; Callis, C. F. *Chem. Rev.* **1958**, *58*, 1011. (b) Clearfield, A. Metal phosphonate chemistry. In *Progress in Inorganic Chemistry*; Karlin, K. D., Ed.; John Wiley & Sons Inc: New York, 1998; Vol. 47, p 371.

(9) Zaitseva, N.; Carman, L. *Prog. Cryst. Growth Charact. Mater.* **2001**, *43*, 1.

(10) Fan, T.-Y.; Huang, C.-E.; Hu, B.-Q.; Eckhardt, R. C.; Fan, Y.-X.; Bayer, R. L.; Feigelson, R. S. *Appl. Opt.* **1987**, *26*, 2391.

(11) Hong, H. Y.-P. *Mater. Res. Bull.* **1975**, *10*, 1105.

(12) (a) Kapakoglou, N. I.; Panagiotis, B. I.; Kazianis, S. E.; Kosmidis, C. E.; Drouza, C.; Manos, M. J.; Sigalas, M. P.; Keramidas, A. D.; Kabanos, T. A. *Inorg. Chem.* **2007**, *46*, 6002. (b) Liu, C.-G.; Guan, W.; Song, P.; Su, Z.-M.; Yao, C.; Wang, E.-B. *Inorg. Chem.* **2009**, *48*, 8115. (c) Kong, F.; Hu, C.-L.; Xu, X.; Zhou, T.-H.; Mao, J.-G. *Dalton Trans.* **2012**, *41*, 5687.

(13) (a) Kierkegaard, P. *Ark. Kemi* **1962**, *18*, 553. (b) Kierkegaard, P.; Holmen, S. *Ark. Kemi* **1965**, *23*, 213. (c) Peascoe, R.; Clearfield, A. J. *Solid State Chem.* **1991**, *93*, 83. (d) Leclaire, A.; Guesdon, A.; Borel, M. *Solid State Sci.* **2002**, *3*, 877.

(14) *SAINT: Program for Area Detector Absorption Correction*, Version 4.05; Siemens Analytical X-ray Instruments: Madison, WI, 1995.

(15) Blessing, R. H. *Acta Crystallogr., Sect. A: Found. Crystallogr.* **1995**, *51*, 33.

(16) Sheldrick, G. M. *SHELXTL*, version 6.12; Bruker Analytical X-ray Instruments, Inc.: Madison, WI, 2001.

(17) Spek, L. *J. Appl. Crystallogr.* **2003**, *36*, 7.

(18) (a) Kubelka, P.; Munk, F. *Z. Tech. Phys.* **1931**, *12*, 593. (b) Tauc, J. *Mater. Res. Bull.* **1970**, *5*, 721.

(19) Kurtz, S. K.; Perry, T. T. *J. Appl. Phys.* **1968**, *39*, 3798.

(20) (a) Fan, X.-Y.; Pan, S.-L.; Hou, X.-L; Liu, G. *Inorg. Chem.* **2009**, 4806. (b) Wang, Y.-J.; Pan, S.-L.; Tian, X.-L.; Zhou, Z.-X.; Liu, G.; Wang, J.-D.; Jia, D.-Z. *Inorg. Chem.* **2009**, *48*, 7800. (c) Li, F.; Pan, S.-L.; Hou, X.-L.; Yao, J. *Cryst. Growth Des.* **2009**, *9*, 4091. (d) Fan, X.-Y.; Pan, S.-L.; Hou, X.-L.; Tian, X.-L.; Han, J.; Haag, J.; Poeppelmeier, K. R. *Cryst. Growth Des.* **2010**, *10*, 252.

(21) Dougherty, J. P.; Kurtz, S. K. *J. Appl. Crystallogr.* **1976**, *9*, 145.

(22) (a) Segall, M. D.; Lindan, P. J. D.; Probert, M. J.; Pickard, C. J.; Hasnip, P. J.; Clark, S. J.; Payne, M. C. *J. Phys.: Condens. Matter* **2002**, *14*, 2717. (b) Milman, V.; Winkler, B.; White, J. A.; Pickard, C. J.; Payne, M. C.; Akhmatskaya, E. V.; Nobes, R. H. *Int. J. Quantum Chem.* **2000**, *77*, 895.

(23) Perdew, J. P.; Burke, K.; Ernzerhof, M. *Phys. Rev. Lett.* **1996**, *77*, 3865.

(24) Lin, J. S.; Qteish, A.; Payne, M. C.; Heine, V. *Phys. Rev. B* **1993**, *47*, 4174.

(25) Baerloch, C.; Meier, W. M. *Helv. Chim. Acta* **1970**, *53*, 1285.

(26) Koch, E.; Fischer, W. *Z. Z. Kristallogr.* **1995**, *210*, 407.

(27) O'Keeffe, M.; Peskov, M. A.; Ramsden, S. J.; Yaghi, O. M. *Acc. Chem. Res.* **2008**, *41*, 1782.

(28) (a) Brese, N. E.; O'Keeffe, M. *Acta Crystallogr., Sect. B: Struct. Sci.* **1991**, *47*, 192. (b) Brown, I. D.; Altermatt, D. *Acta Crystallogr., Sect. B: Struct. Sci.* **1985**, *41*, 244.

(29) Chang, H.-Y.; Kim, S. H.; Ok, K. M.; Halasyamani, P. S. *J. Am. Chem. Soc.* **2009**, *131*, 6865.

(30) Strandberg, R. *Acta Chem. Scand.* **1973**, *27*, 1004.

(31) (a) Cao, X.-G.; He, L.-W.; Lin, B.-Z.; Xiao, Z.-J. *J. Chem. Crystallogr.* **2010**, *40*, 443. (b) Dey, C.; Kundu, T.; Banerjee, R. *Chem. Commun.* **2012**, *48*, 266. (c) Cao, R.; Liu, S.; Cao, J.; Wang, L.; Tang, Q.; Liu, Y.; Ren, Y. *J. Mol. Struct.* **2008**, *888*, 307. (d) Lin, B.-Z.; Li, Z.; Xu, B.-H.; He, L.-W.; Liu, X.-Z.; Ding, C. *J. Mol. Struct.* **2006**, *825*, 87.

(32) (a) Maggard, P. A.; Nault, T. S.; Stern, C. L.; Poeppelmeier, K. R. *J. Solid State Chem.* **2003**, *175*, 27. (b) Ok, K. M.; Halasyamani, P. S. *Inorg. Chem.* **2005**, *44*, 3919. (c) Kim, J. H.; Halasyamani, P. S. *J. Solid State Chem.* **2008**, *181*, 2108.

(33) Li, C.-H.; Huang, K.-L.; Chi, Y.-N.; Liu, X.; Han, Z.-G.; Shen, L.; Hu, C.-W. *Inorg. Chem.* **2009**, *48*, 2010.

(34) (a) Brown, I. D. *The Chemical Bond in Inorganic Chemistry: The Bond Valence Model*, 1st ed.; Oxford University Press: Oxford, U.K., 2002. (b) Preiser, C.; Lösel, J.; Brown, I. D.; Kunz, M.; Skowron, A. *Acta Crystallogr., Sect. B: Struct. Sci.* **1999**, *55*, 698. (c) Salinas-Sanchez, A.; Garcia-Muñoz, J. L.; Rodriguez-Carvajal, J.; Saez-Puche, R.; Martinez, J. L. *J. Solid State Chem.* **1992**, *211*, 201.

(35) (a) Kwak, W.; Pope, M. T.; Scully, T. F. *J. Am. Chem. Soc.* **1975**, *97*, 5735. (b) Nyquist, R. A.; Kagel, R. O. *Infrared Spectra of Inorganic Compounds*; Academic Press: New York, 1971. (c) Zhang, C.-X.; Chen, Y.-G.; Tang, Q.; Zhang, Z.-C.; Liu, D.-D.; Meng, H.-X. *Inorg. Chem. Commun.* **2012**, *17*, 155. (d) Himeno, S.; Ueda, T.; Shiomi, M.; Hori, T. *Inorg. Chim. Acta* **1997**, *262*, 219. (e) Mooney, R. W.; Goldsmith, R. L. *J. Inorg. Nucl. Chem.* **1969**, *31*, 933. (f) Wang, Y.; Pan, S.-L.; Shi, Y.-J. *Chem.—Eur. J.* **2012**, *18*, 12046.

(36) (a) Terki, R.; Bertrand, G.; Aourag, H. *Microelectron. Eng.* **2005**, *1*, 514. (b) Okoye, C. M. I. *J. Phys.: Condens. Matter* **2003**, *15*, 5945. (c) Godby, R. W.; Schluther, M.; Sham, L. *J. Phys. Rev. B* **1987**, *36*, 6497.